






Article

Mpro-SARS-CoV-2 Inhibitors and Various Chemical Reactivity of 1-Bromo- and 1-Chloro-4-vinylbenzene in [3 + 2] Cycloaddition Reactions

Mohammed El Idrissi^{1,2}, Mohamed El Ghazlani³, Asli Eşme⁴ , Mar Ríos-Gutiérrez⁵ , Anas Ouled Aitouna¹, Mohammed Salah¹, Habib El Alaoui El Abdallaoui¹, Abdellah Zeroual^{1,*} , Nouredine Mazoir⁶  and Luis R. Domingo⁵ 

- ¹ Molecular Modeling and Spectroscopy Research Team, Faculty of Science, Chouaib Doukkali University, El Jadida 24000, Morocco; m.elidrissi2018@gmail.com (M.E.I.); anas.ouledaitouna@edu.uca.ac.ma (A.O.A.); salahmed534@gmail.com (M.S.); elalaoui.habib@yahoo.fr (H.E.A.E.A.)
- ² Laboratory of Chemical Processes and Applied Materials, Polydisciplinary Faculty, Sultan Moulay Slimane University, Beni-Mellal 23000, Morocco
- ³ Organic and Analytical Chemistry Laboratory, Faculty of Science and Technology, Sultan Moulay Slimane University, Beni-Mellal 23000, Morocco; elghozlanimohamed@gmail.com
- ⁴ Department of Elementary Science Education, Faculty of Education, Kocaeli University, Kocaeli 41380, Turkey; asliesme@gmail.com
- ⁵ Department of Organic Chemistry, University of Valencia, Dr. Moliner 50, 46100 Valencia, Spain; rios@utopia.uv.es (M.R.-G.); domingo@utopia.uv.es (L.R.D.)
- ⁶ Department of Organic Chemistry, Faculty of Sciences, Chouaib Doukkali University, El Jadida 24000, Morocco; mazoirm@gmail.com
- * Correspondence: zeroualabdellah2@gmail.com



Citation: El Idrissi, M.; El Ghazlani, M.; Eşme, A.; Ríos-Gutiérrez, M.; Ouled Aitouna, A.; Salah, M.; El Abdallaoui, H.E.A.; Zeroual, A.; Mazoir, N.; Domingo, L.R. Mpro-SARS-CoV-2 Inhibitors and Various Chemical Reactivity of 1-Bromo- and 1-Chloro-4-vinylbenzene in [3 + 2] Cycloaddition Reactions. *Organics* **2021**, *2*, 1–16. <https://doi.org/10.3390/org2010001>

Received: 21 October 2020

Accepted: 21 December 2020

Published: 4 January 2021

Publisher's Note: MDPI stays neutral with regard to jurisdictional claims in published maps and institutional affiliations.



Copyright: © 2021 by the authors. Licensee MDPI, Basel, Switzerland. This article is an open access article distributed under the terms and conditions of the Creative Commons Attribution (CC BY) license (<https://creativecommons.org/licenses/by/4.0/>).

Abstract: The regioselectivity and the mechanism of the (32CA) cycloadditions reactions of 1-bromo-4-vinylbenzene **1** and 1-chloro-4-vinylbenzene **2** with benzonitrile oxide **3** were investigated under the molecular electron density theory (MEDT) at the B3LYP/6-311++G(d,p) computational level. Evaluation of the ELF reveals that these zwitterionic type (*zw-type*) 32CA reactions take place in a *two-stage one-step* mechanism. This MEDT study shows that the *meta* isoxazolines are kinetically and thermodynamically favored over the *ortho* ones, these 32CA reactions being completely regioselective, in agreement with experimental outcomes. In addition, the efficiency of isoxazolines against SARS-CoV-2 have been also investigated. According to the docking analysis, the present study concludes that 5-(*p*-bromophenyl)-3-phenyl-2-isoxazoline (**B-m**) shows better interactions for the inhibition of SARS-CoV-2 in comparison to chloroquine.

Keywords: 2-isoxazoline; MEDT; regioselectivity; SARS-CoV-2; DFT; ELF

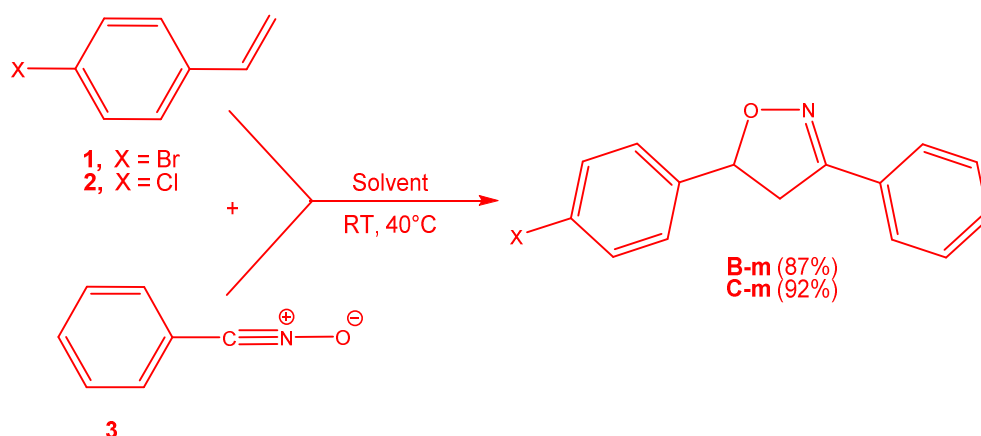
1. Introduction

A heterocyclic compounds constitute the basic skeleton for a wide variety of species of chemical, biological, pharmacological, and industrial interest [1,2]. As a result, heterocyclic chemistry has become the focus of a large community of experimental and theoretical chemists. One of the most used methods to prepare heterocycles is the [3 + 2] cycloaddition (32CA) reaction; the principal conception and the mechanism of 32 CA reactions were formulated by Huisgen and Firestone [3–7]. Nitrile oxides are known to be very good reagents in 32CA reactions; they react with a wide variety of ethylene derivatives, such as α , β -unsaturated carbonyl compounds, enals, or alkenes. The 32CA reaction between nitrile oxides and alkenes leads to the formation of isoxazolines, which are 5-membered heterocyclic compounds comprising contiguous oxygen and nitrogen atoms, as well as a C–N double bond on nitrogen. The isoxazoline is of valuable interest in several fields as biology. Indeed, 2-isoxazolines compounds possess biological activity [8], such as with antifungal [9], antiviral [10], antitumor [11], anticancer [12], Anti-HIV-RT [13],

anti-inflammatory [14] and antimicrobial properties [15,16]. The introduction of halogen atoms into isoxazolines has an effect on its physical and chemical properties, allowing interesting and useful properties to appear in various pharmaceutical fields. Consequently, the introduction of a fluoride, chlorine, or bromine functionality in isoxazolines has attracted considerable interest from the synthetic community [17–37], because they are very promising as products for medical applications [38–40].

Progress in the theoretical comprehension of 32 CA reactions founded on molecular electron density theory [41] (MEDT) shows a relationship between the electronic structure of the simplest three-atom components (TAC) and their reactivity ethylene [42]. Thus, depending of the structure of the TACs, *pseudodiradical*, *pseudoradical*, carbenoid or zwitterionic, 32CA reactions have been classed as *pseudodiradical type (pdr-type)*, *pseudoradical type (pmr-type)*, carbenoid type (*cb-type*) and zwitterionic type (*zw-type*) [42–45], in such a manner that while *zw-type* 32CA reactions demand high activation energies to take place, while *pdr-type* 32CA reactions can be carried out without difficulty [42].

Herein, a MEDT study of the 32CA reaction of 1-bromo-4-vinylbenzene (BrVB) **1**, and 1-chloro-4-vinylbenzene (ClVB) **2** with benzonitrile oxide (BzNO) **3**, experimentally studied by Yoshimura [46], is carried out in order to understand the molecular mechanism and the regioselectivity of these reactions (Scheme 1). Given the broad activities of isoxazolines [46], we now wanted to investigate their potential inhibition by interaction with Mpro proteases of virus.



Scheme 1. 32CA reaction of BrVB **1**, ClVB **2** and BzNO **3**.

2. Computational Methods

DFT computations were performed using the B3LYP [47] and 6-311++G(d,p) basis set [48], with the Gaussian 09 package [49]. Berny's analytical gradient optimization method was used in the optimizations [50]. Frequency calculations were performed at located stationary points to ensure that the TSs only had one imaginary frequency. The intrinsic reaction coordinate (IRC) [51] calculations using González-Schlegel integration method [52] were used to verify the minimum energy reaction pathway connecting the reactants and the products. Solvents influences of tetrahydrofuran (THF) were envisioned using the Continuous Polarization Model (PCM) developed by the Tomasi's group [53] in the framework of the self-consistent reaction field (SCRF) [54].

The global electron density transfer [55] (GEDT) was computed from natural population analysis (NPA) [56], of the atoms belonging to each framework (f) at the TSs; i.e., $\text{GEDT}(f) = \sum_{q \in f} q$. The sign indicates the direction of the electron density flux in such a manner that positive values mean a flux from the considered framework to the other one. The Conceptual DFT (CDFT) reactivity indices [57] were computed using the equations given in reference [57]. The electron localization function (ELF) [58] was performed using the TopMod program [59,60].

Finally, to test the asynchronicity in the studied reactions, we have analyzed the independent gradient model (IGM) [61] based on the electron density (ED), which is more physically significant for chemical bonding analysis [62]. Indeed, the independent gradient model approach (IGM), is more qualified to evaluate the evolution of the formation of new bonds. The IGM is very efficient to reveal the covalent bonding pattern and visualize the weak interactions where other tools were visibly failing [63]. This is done through the mono determinantal wave functions of the ground state (GS) and that of the transition structures calculated at B3LYP/6-311++G(d,p) level, using the Multiwfn software [64]. The physical descriptor associated with IGM [61] is symbolized by δg , $\delta g = |\nabla \rho^{\text{IGM}}| - |\nabla \rho|$. ρ represents the electron density (this is a local function), and is an experimentally accessible scalarfield, $|\nabla \rho^{\text{IGM}}|$ represents the virtual upper limit of the electron density gradient and $|\nabla \rho|$ represents a non-interacting system electron density gradient. δg is a measure of the ED gradient collapse caused by electron sharing between contra gradient ED sources present in the chemical system.

3. Results and Discussion

This MEDT study was divided into five parts: (i) primary, an ELF study of the electronic structure of BrVB **1**, CIVB **2** and BzNO **3** is presented; (ii) in the next part, the CDFT reactivity indices of the reagents are analyzed; (iii) in the third part, the competitive reaction paths associated with the 32CA reactions of BrVB **1** and CIVB **2** with BzNO **3** are investigated; (iv) in the fourth part, the formation of the new single bonds along the most favorable reaction path are described through the topological analysis of the ELF; and finally (v) in the fifth part, molecular docking studies were carried out to explore the activities of the isoxazolines for the main protease of Coronavirus disease (COVID-19).

3.1. ELF Analysis of the Electronic Structure of BrVB **1**, CIVB **2** and BzNO **3**

Recently, an appealing correlation between the reactivity and the electronic structure of simplest TACs contributing in 32CA reactions toward ethylene was established [42]. ELF, first constructed by Becke and Edgecombe [58] and further illustrated by Silvi and Savin [65], permits establishing a straightforward quantitative connection between the electron density distribution and the chemical structure. Therefore, a topological analysis of the ELF of BrVB **1**, CIVB **2** and BzNO **3** was performed in order to predict their structure and reactivity in 32CA reactions [42]. The ELF attractor positions, the ELF localization domains and the proposed Lewis-like structures of BrVB **1**, CIVB **2** and BzNO **3**, together with the natural atomic charges, are shown in Figure 1.

Topological analysis of the ELF of BrVB **1** shows six disynaptic basins associated with the aromatic ring, with a total population of 16.81 e, and three disynaptic basins, V (C1,C2), V' (C1,C2) and V (C2,C3), integrating 1.73, 1.63 and 2.24 e, respectively, associated with the C2-C1 double bond and the C3-C2 single bond, as well as two V(Br) monosynaptic basins carried by the bromine atom, integrating of 6.66 e. Similarly, ELF for CIVB **2** reveals the presence of six disynaptic basin associated with the aromatic ring, integrating a total of 16.84 e, and three disynaptic basins, V(C1',C'2), V'(C1',C'2) and V (C2',C3'), integrated 1.69, 1.68 and 2.24 e, respectively, associated with the C2'-C1' double bond and the C3'-C2' the simple bond, respectively. In addition, two V(Cl) monosynaptic basins carried by the chlorine atom, integrating 6.35 e, are observed. The topological analysis of the ELF of BzNO **3** shows the presence of two V(C4,N) and V'(C4,N) disynaptic basins, integrating a total of 5.74 e, associated with the C4-N triple bonding regions, a V(O,N) disynaptic basins, integrating of 1.28 e, associated with the depopulated O-N single bond, and two V(O) monosynaptic basins, integrating a total of 5.68 e, related to the non-bonding region of the O oxygen, as well as six disynaptic basins, integrating 16.57 e, related with the aromatic ring. Therefore, ELF of BzNO **3** indicates that it has a propargylic linear structure associated with a zwitterionic TAC participating in *zw-type* 32CA reactions. These TACs have moderately low regioselectivity and low reactivity [42].

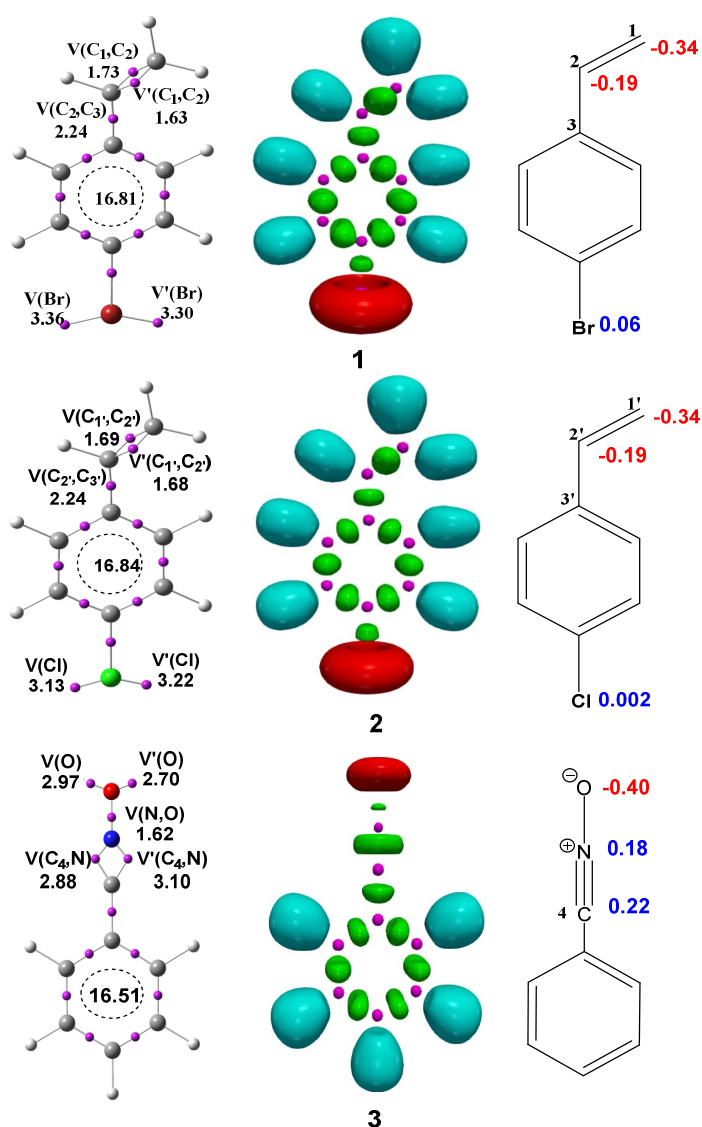


Figure 1. B3LYP/6-311++G (d,p) ELF basin attractor positions, together with the valence basin populations, ELF localization domains, represented at an isosurface value of ELF = 0.75, and natural atomic charges, of BrVB **1**, CIVB **2** and BzNO **3**. Negative charges are colored in red and positive charges in blue. ELF valence basin populations and natural atomic charges are given on average number of electrons, e.

3.2. Analysis of CDFT Reagent Indices

The reactivity of the reagents involved in these 32CA reactions, BrVB **1**, CIVB **2**, and BzNO **3**, was studied, by analyzing the CDFT reactivity indices [57]. The chemical hardness η , the electronic chemical potential μ , the electrophilicity ω and nucleophilicity N indices are given in Table 1.

Table 1. B3LYP/6-31G(d) chemical hardness η , electronic chemical potential μ , electrophilicity ω , and nucleophilicity N indices, in eV, of BrVB **1**, CIVB **2** and BzNO **3**.

System	η	μ	ω	N
BrVB 1	4.97	−3.63	1.32	3.41
CIVB 2	5.02	−3.64	1.32	3.36
BzNO 3	5.02	−3.82	1.45	3.19

The electronic chemical potentials μ [66] of BrVB **1**, -3.63 eV and CIVB **2**, -3.64 eV, are only slightly higher than that of BzNO **3**, -3.82 eV. The very close electronic chemical potentials μ of these species indicate that these 32CA reactions will have a very low polar character. Likewise, these compounds present very similar chemical hardness η values, ca. 5 eV.

The electrophilicity [67] ω and nucleophilicity [68] N indices of BrVB **1** are 1.32 and 3.41 eV, respectively, and those of CIVB **2** are 1.32 and 3.36 eV, respectively, allowing their classification as moderate electrophiles and strong nucleophiles [69]. The electrophilicity ω and nucleophilicity N indices of BzNO **3**, are 1.45 and 3.19 eV, respectively, allowing its classification as a moderate electrophile and a strong nucleophile. The moderate electrophilic character of the three reagents indicates that these *zw-type* 32CA reactions will have low polar character. In addition, the slightly higher nucleophilic character of BrVB **1** and CIVB **2** than BzNO **3**, and the slightly higher electrophilic character of BzNO **3** than BrVB **1** and CIVB **2**, suggest that along these 32CA reactions, BrVB **1** and CIVB **2** will participate as the nucleophile, while BzNO **3** will participate as the electrophile.

Along a polar reaction engaging the contribution of non-symmetric reagents, the most favorable reactive channel is that involving the initial two-center interaction between the most electrophilic center of the electrophile and the most nucleophilic center of the nucleophile [70]. In this context, the electrophilic P_k^+ and nucleophilic P_k^- Parr functions [71] derived from the excess of spin electron density reached via the GEDT [55] process from the nucleophile toward the electrophile have shown to be the most accurate and insightful tools for the study of the local reactivity in polar and ionic processes. The Parr functions as well as the maps of the atomic spin density (ASD) of the ions, the radical anion of BrVB **1** and CIVB **2**, and of the radical cation of BzNO **3** are given in Figure 2.

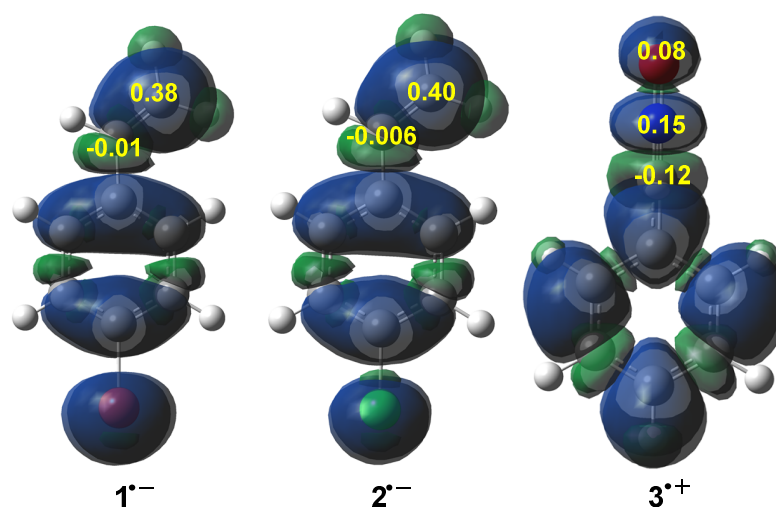
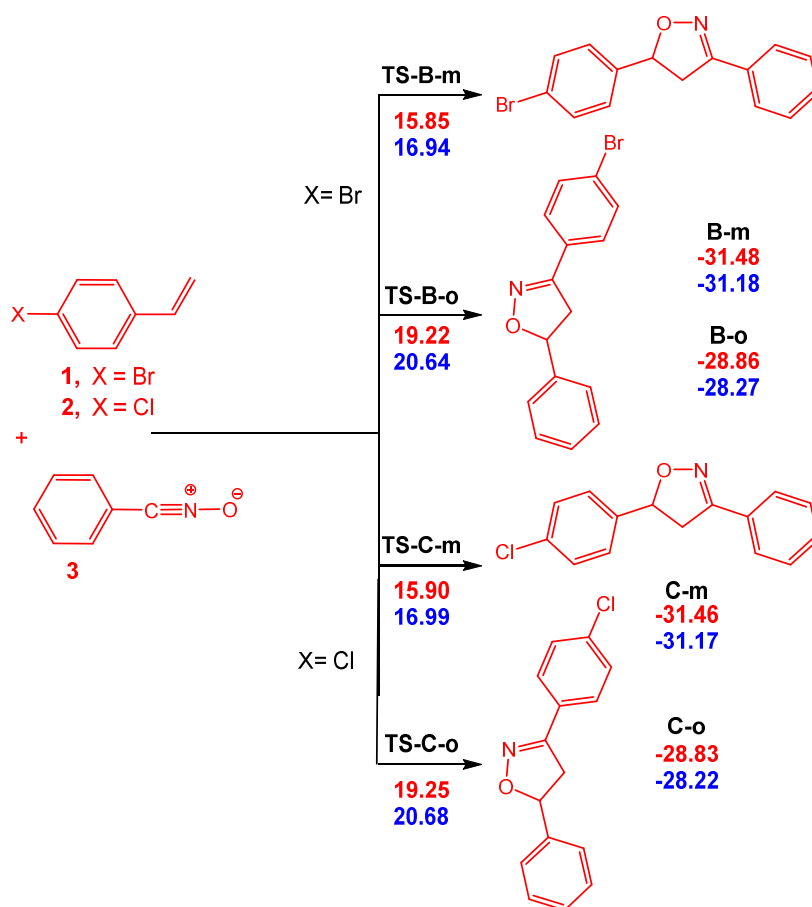


Figure 2. 3D representations of the Mulliken ASDs of the radical cations together with the nucleophilic P_k^- Parr functions of BrVB **1** and CIVB **2**, and the Mulliken ASDs of radical anion together with the electrophilic P_k^+ Parr functions of BzNO **3**.

Analysis of the nucleophilic P_k^- Parr functions of BrVB **1** and CIVB **2** indicates that the terminal carbon of the C-C double bond is the most nucleophilic center of these species, 0.38 and 0.40, respectively. On the other hand, the C-N-O framework of BzNO **3** has small electrophilic P_k^+ Parr function values, lower than 0.1, because they are gathered at the phenyl ring. Consequently, the analysis of the electrophilic P_k^+ Parr functions indicates that BzNO **3** will have a poor participation in polar *zw-type* 32CA reactions, in clear agreement with the high activation energy found at the most favorable **TS-B-m** and **TS-C-m** (see below).

3.3. Exploration of the Reaction Paths Associated with 32CA Reaction of BrVB 1 and CIVB 2 with BzNO 3

The experimental formation of the *meta* isoxazolines **B-m** and **C-m**, which are the main cycloadducts, indicates that these 32CA reactions present complete regioselectivity [46]. Due to the non-symmetry of the reagents two competitive regioisomeric reaction paths are feasible for these 32CA reactions, the *ortho* and the *meta*. Two regioisomeric isoxazolines and the corresponding TSs were located and identified along each reaction paths (see Scheme 2). Consequently, these 32CA reactions take place through a one-step mechanism. The relative energies, in THF and gas, for the different stationary points in their ground state are given in Scheme 2, while the total electronic energies are provided in Table S1 in Supporting Information. The frequencies and the Cartesian coordinates of the TSs are also given in Supporting Information.



Scheme 2. The two regioisomeric reaction paths associated with the 32CA reactions of BrVB 1 and CIVB 2 with BzNO 3. DFT/B3LYP/6-311++G(d,p) relative energies, in gas phase (in red) and in THF (in blue), are given in kcal·mol⁻¹.

Scheme 2 shows that the TSs associated with the *meta* reaction paths, 15.85 (TS-B-m) and 15.90 (TS-C-m) kcal·mol⁻¹, are 3.37 and 3.35 kcal·mol⁻¹, respectively, lower in energy than the *ortho* TSs. Formation of the corresponding isoxazolines is very exothermic between 28.22 (C-o) and 31.18 (B-m) kcal·mol⁻¹. On the other hand, the *meta* isoxazolines **B-m** and **C-m**, -31.48 and -31.46 kcal·mol⁻¹, respectively, are more stable than the *ortho* ones **B-o** and **C-o**, -28.86 and -28.83 kcal·mol⁻¹, respectively. Consequently, formation of the *meta* isoxazolines **B-m** and **C-m** is both kinetically and thermodynamically favored over the *ortho* ones, in complete agreement with the experimental results [46]. To study the solvent effects along the reaction paths, the solvent THF was taken into account. The activation energies of these reaction paths slightly increase and their exothermic character slightly decrease

with the inclusion of solvent effects. These findings are an effect of an ameliorate solvation of the reagents than isoxazolines and TSs. The Gibbs free energy and enthalpy profiles of the reaction paths associated with the 32CA reactions of BrVB 1 and CIVB 2 with BzNO 3 are given in Figure 3, while the thermodynamic data is prearranged in Table S2 (ESI).

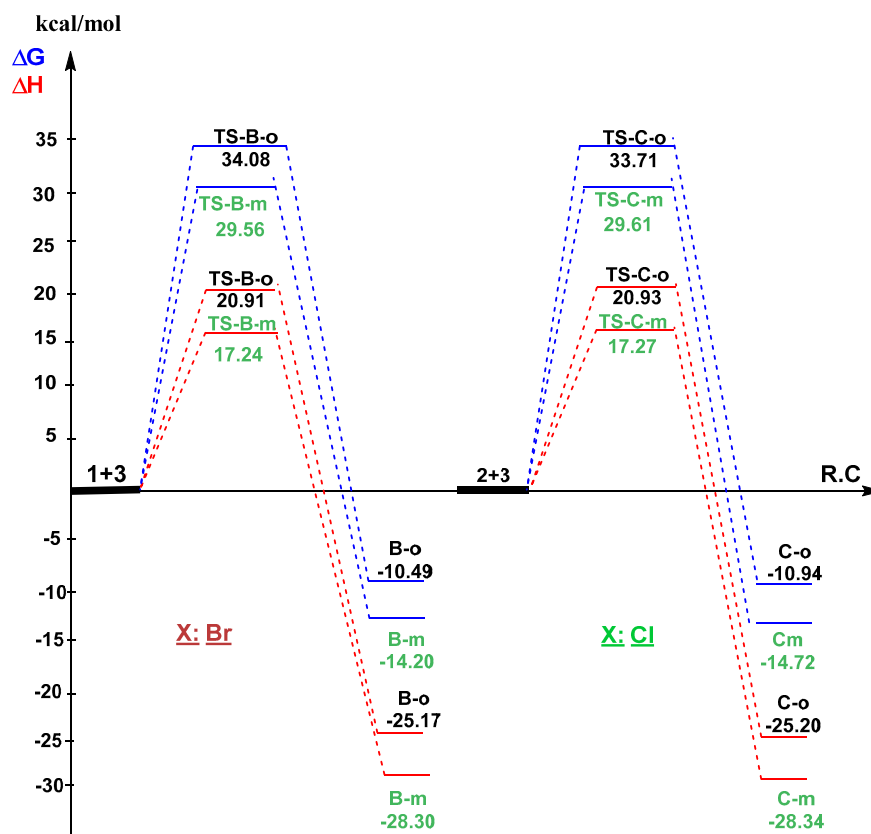


Figure 3. Gibbs free energy (ΔG in blue) and enthalpy (ΔH in red) profile, for the studied reaction paths of the 32CA reactions of BrVB 1 and CIVB 2 with BzNO 3, in THF at 25 °C.

The inclusion of the entropy and temperature toward the enthalpy noticeably increases the activation Gibbs free energies, by between 12 and 14 kcal·mol⁻¹, and significantly decreases the reaction Gibbs free energies, by between 13 and 15 kcal·mol⁻¹, due to the unfavorable entropy associated with these bimolecular processes. The activation Gibbs free energies related with the formation of **B-m**, **B-o**, **C-m** and **C-o** are 29.56, 34.08, 29.61 and 33 kcal·mol⁻¹, respectively. The activation free Gibbs energies also show a total regioselectivity. These 32CA reactions are exergonic between 10.49 (**B-o**) and 28.34 (**C-m**) kcal·mol⁻¹, indicating that the formation of the isoxazolines **B-m** and **C-m** is thermodynamically irreversible.

The optimized geometries, in THF and gas, of the TSs associated with the 32CA reactions of BrVB 1 and CIVB 2 with BzNO 3 are shown in Figure 4. Along the *meta* reaction paths, the distances associated with the formation of new O-C and C-C single bonds are 2.459 and 2.177 Å at **TS-B-m**, and 2.461 and 2.177 Å at **TS-C-m**, respectively, while along the *ortho* reaction paths, these distances are 2.147 and 2.231 Å at **TS-B-o**, and 2.162 and 2.220 Å at **TS-C-o**, respectively. Taking into account that the formation of C-C single bonds takes place in the range of 2.00–1.90 Å, and that the formation of C-O single bonds takes place in the range of 1.80–1.70 Å, [42] these distances indicate that the formation of neither C-C nor C-O single bonds have yet begun at the four TSs. In addition, the C-C and C-O distances at the more favorable *meta* TSs show that they are associated with highly asynchronous mechanisms. Indeed, the IGM calculations suggest that the formation of the C-C single bond ($\delta g = 0.37$) is more advanced than that of the C-O one ($\delta g = 0.23$), which confirms an asynchronicity in the case of **TS-B-m** and **TS-C-m** (Figure 4).

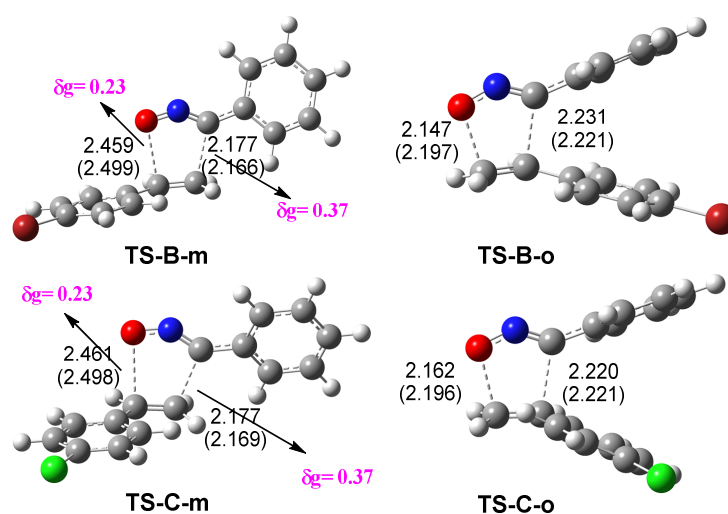


Figure 4. B3LYP/6-311++G(d,p) optimized geometries of the TSs involved in the two regioisomeric reaction pathways associated with the 32CA reactions of BrVB **1** and CIVB **2** with BzNO **3** and IGM values (δg). Distances are given in angstroms, Å. Distances in THF are given in parentheses.

We also noted that the molecular entity BzNO containing the phenyl group tends to perform a rotation caused by the steric hindrance associated with phenyl group of CIVB and BrVB in the case of TS-B-O and TS-C-O (Figure 4).

To evaluate the polar nature of these 32CA reactions, the GEDT [55] at the TSs was analyzed. 32CA reactions with GEDT values below 0.05 e correspond to non-polar processes, while values above 0.2 e correspond to polar processes. The GEDT values measured at the TAC framework of the four TSs are 0.03 e at **TS-B-m**, 0.03 e at **TS-B-o**, 0.04 e at **TS-C-m** and 0.03 e at **TS-C-o**. These very low GEDT values (lower than 0.05 e), account for the non-polar character of these *zw-type* 32CA reactions, in complete agreement with the analysis of the CDFT indices.

3.4. Bonding Evolution Theory (BET) Study of the 32CA Reactions of BrVB **1** and CIVB **2** with BzNO **3**

To understand the bonding changes along the *meta* regioisomeric reaction paths associated with the 32CA reactions of BrVB **1** and CIVB **2** with BzNO **3**, a BET study [60] was carried out. BET is very useful tool to characterize the bonding changes along a reaction path and, therefore, to determine the nature of the electronic rearrangement associated with a molecular mechanism. A topological analysis of the ELF of the structures along the IRC involved in the studied 32CA reaction was carried out in order to describe the formation/breaking of the bonds. The most relevant bond distances and populations of the most significant ELF valence basins are gathered in Tables S3 and S4 in Supporting Information. A detailed description of the BET analysis is given in Supporting Information, together with a simplified representation of the molecular mechanism of the 32CA reactions in Figures S1 and S2 and Scheme S1, while the most relevant conclusions obtained from this BET analysis are summarized below.

From the BET study the following appealing conclusions can be obtained: (i) the IRC associated with the 32CA reactions of BrVB **1** and CIVB **2** with BzNO **3** are divided into fourteen phases, which clearly indicates that the behavior of these one-step mechanism is non-concerted; (ii) the reaction begins with the depopulation of the N-C triple bond of BzNO **3**. This feature is identical to that found in the 32CA reaction between acetonitrile N-oxide and 2,5-dimethyl-2H-[1-3] diazarsole [72]; (iii) formation of the C1 *pseudoradical* center takes place in *Phase I* (**B-1**) and (**C-2**), while the formation of the C3 *pseudoradical* center begins in the same *Phase I* (**B-4**) and (**C-4**); (iv) formation of the first C1-C3 single bond begins in **B-7** and **C-5**, by sharing the non-bonding electron density of the two C1 and C3 *pseudoradical* carbons; (v) formation of the second O-C2 single bond begins at the

end of the reaction paths in *Phases IX* and *X*, at a O-C2 distance of 2.14 Å for the 32CA reaction of BrVB **1**, and 2.13 Å for the 32CA reaction of ClVB **2**, via the donation of part of the non-bonding electron density of oxygen O of the NO framework to C2 carbon of these alkenes; (vi) these behaviors make it possible to conclude that these *zw-type* 32CA reactions follow a non-concerted *two-stage one-step* mechanism [73], as the formation of the second O-C single bond begins after the formation of about 90% of the first C1-C3 single bond.

3.5. Molecular Docking

The isoxazole structures considered as potential pharmacological agents constitute the most promising five-membered heterocyclic units [74]. Some isoxazoles and related compounds are known to exhibit antitumor [75], anti-HIV [76], anti-inflammatory [77], antioxidant [78], antiviral [79], antimicrobial activities [80] and insecticidal [81]. Currently, there is no approved drug for the treatment of coronaviral disease, although Chloroquine has in vitro activity against SARS-CoV-2. The COVID-19 is a disease caused by severe acute respiratory syndrome coronavirus-2 (SARS-CoV-2). The present section aims to investigate the potential inhibition of the 5-(substituted-phenyl)-3-phenyl-2-isoxazoline derivatives against Mpro of SARS-CoV-2. Furthermore, we have compared between our products and Chloroquine about their ability of interaction with the Mpro. Technically, the parameters adopted for docking are as follow, the number of GA runs: 50, the population size: 300, maximum number of energy evaluations: 2,500,000 (medium), maximum number of generations: 27,000, All other parameters, such as the rate of gene mutation (0.02), and rate of crossover (0.8), were set to defaults. The grid size was chosen as 60 × 60 × 60 with the spacing of 0.5 Å. The center grid box values were set to x = -58.701, y = 10.145, and z = 17.662. Concerning our sample, we have considered a set of 4 molecules with the electron-releasing (CH₃) and electron-withdrawing (Cl, Br, CF₃) groups, computationally optimized by using Gaussian 09 software. The main proteases (Mpro; PDB ID: 5R7Y, 6LU7) of SARS-CoV-2 virus used to cleave polyproteins into replication-related proteins were obtained from the RCSB Protein Data Bank [82,83]. Molecular docking studies were used to explore the activities of the studied compounds (**D-m**, **C-m**, **B-m**, and **A-m** see Table 2) for the main protease of SARS-CoV-2 [83], using the Auto Dock Tools 1.5.6 [84]; Discovery Studio Visualizer software was used to visually verify the docked compounds and 2D structures of docked ligand compounds with Mpro proteases [85]. Then protein was prepared by removing their water atoms, polar hydrogen atoms were added to the protein, and atomic charges were also estimated using Kollman–Gasteiger scheme [86]. Grid box (60 Å × 60 Å × 60 Å and 40 Å × 40 Å × 40 Å) for 5R7Y and 6LU7 of the Mpro proteases was used in the docking investigating by utilizing the AutoDock Tools using the Lamarckian Genetic Algorithm [87]. The results of 4 ligands docking with the Mpro protease and comparison with the Chloroquine as an antimalarial drug are listed in Table 2. The 2D and 3D structures of docked ligand compounds with Mpro protease (comparison with the Chloroquine) are shown in Figure 5 and Figure 6. The calculated binding energies of the investigated **D-m**, **C-m**, **B-m**, **A-m** compounds (Table 2) interacting with 5R7Y and 6LU7 proteins are in the range of -6.63, -7.03 kcal·mol⁻¹ and -5.59, -6.41 kcal·mol⁻¹ in the order of **B-m** > **C-m** > **D-m** > **A-m** and **B-m** > **C-m** > **A-m** > **D-m**, Table 2, respectively. It could be seen from Figure 5 that the oxygen atom and carbon atom of isoxazoline ring of the **D-m**, **C-m**, **B-m**, **A-m** compounds are interacting with the 5R7Y protein through Conventional Hydrogen Bond interactions with the Arg-4 residue at a distance of ~1.9Å and through a p-Alkyl interaction with Lys-5 residue, respectively. The CH₃, Cl, Br halogens of **D-m**, **C-m**, **B-m**, compounds interact through p-alkyl (methyl, chlorine and bromine) interactions with TYR-126, Pro-293 and Ile-249 residues at distances of 4.6 Å, ~3.4 Å and 5.9, 5.3 Å, respectively which indicates another type of interactions different to hydrogen bond (Non-conventional interactions), associated with van der Waals interactions. The NH and Cl interaction results of Chloroquine and SARS-CoV-2 main protease 5R7Y show conventional hydrogen bond interactions with the PHE-3 residue and p-alkyl interactions with the PHE-291 and LYS-5 residues, respectively. According to the analysis of docking results, the present

study concludes that the 5-(*p*-Bromophenyl)-3-phenyl-2-isoxazoline (**B-m**), which shows better interactions for the inhibition of Mpro of SARS-CoV-2 in comparison to Chloroquine. Isoxazoline **A-m** compound was considered due to its potential to interact with the amino acids, just as F halogen in the electron-withdrawing CF₃ group interacts through halogen (Fluorine) bonding with TYR-126 and PRO-108 residues at distances of 2.9 Å and 5.5 Å, respectively. Additionally, the isoxazoline **A-m** interactions with 5R7Y/6LU7 proteins show conventional hydrogen bond interactions with Arg-4 and Lys-5/THR-292 amino acids, at distances of 1.9/2.9 Å (Figure 5). Moreover, the docking score of chloroquine (−6.28 and −4.36 kcal·mol^{−1}) is lesser than **B-m** (−6.91 and −5.59 kcal·mol^{−1}), **C-m** (−6.98 and −6.21 kcal·mol^{−1}), **B-m** (−7.03 and −6.41 kcal·mol^{−1}), **A-m** (−6.63 and −5.99 kcal·mol^{−1}) enlisted in Table 2.

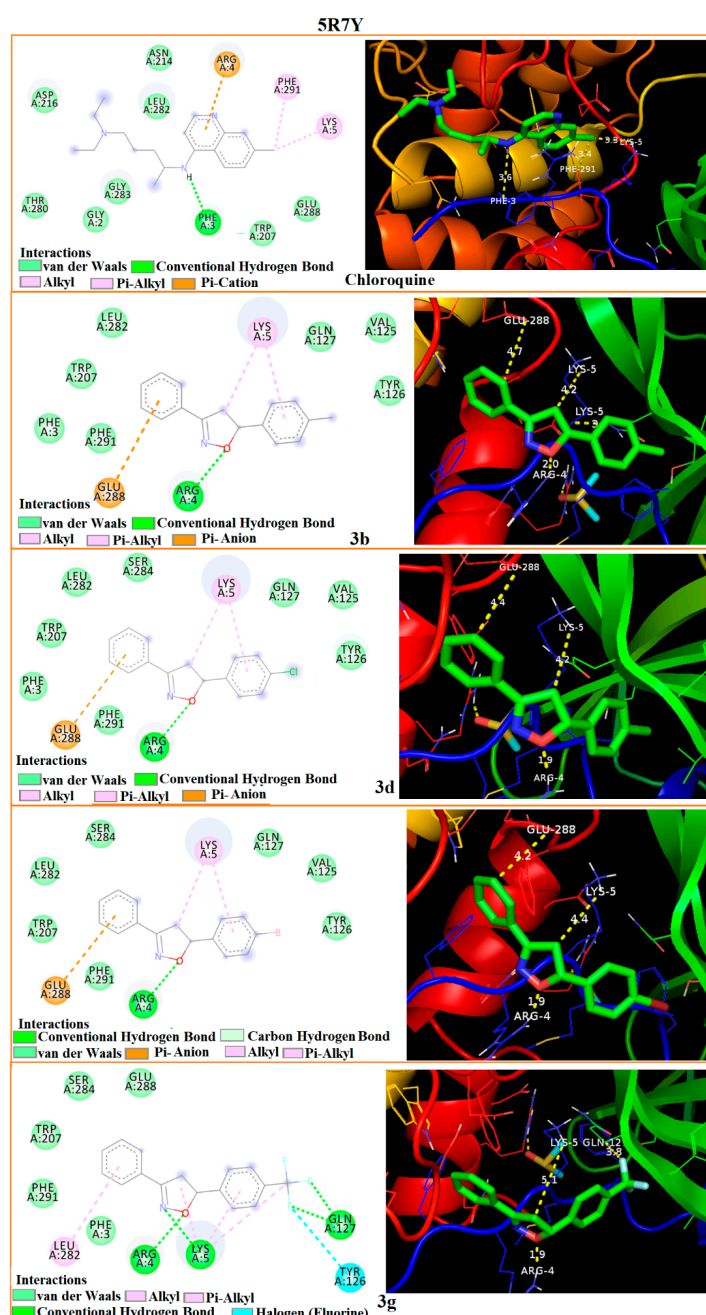


Figure 5. Binding orientation and molecular interactions of the studied **D-m**, **C-m**, **B-m**, **A-m** compounds into the active sites of 5R7Y.

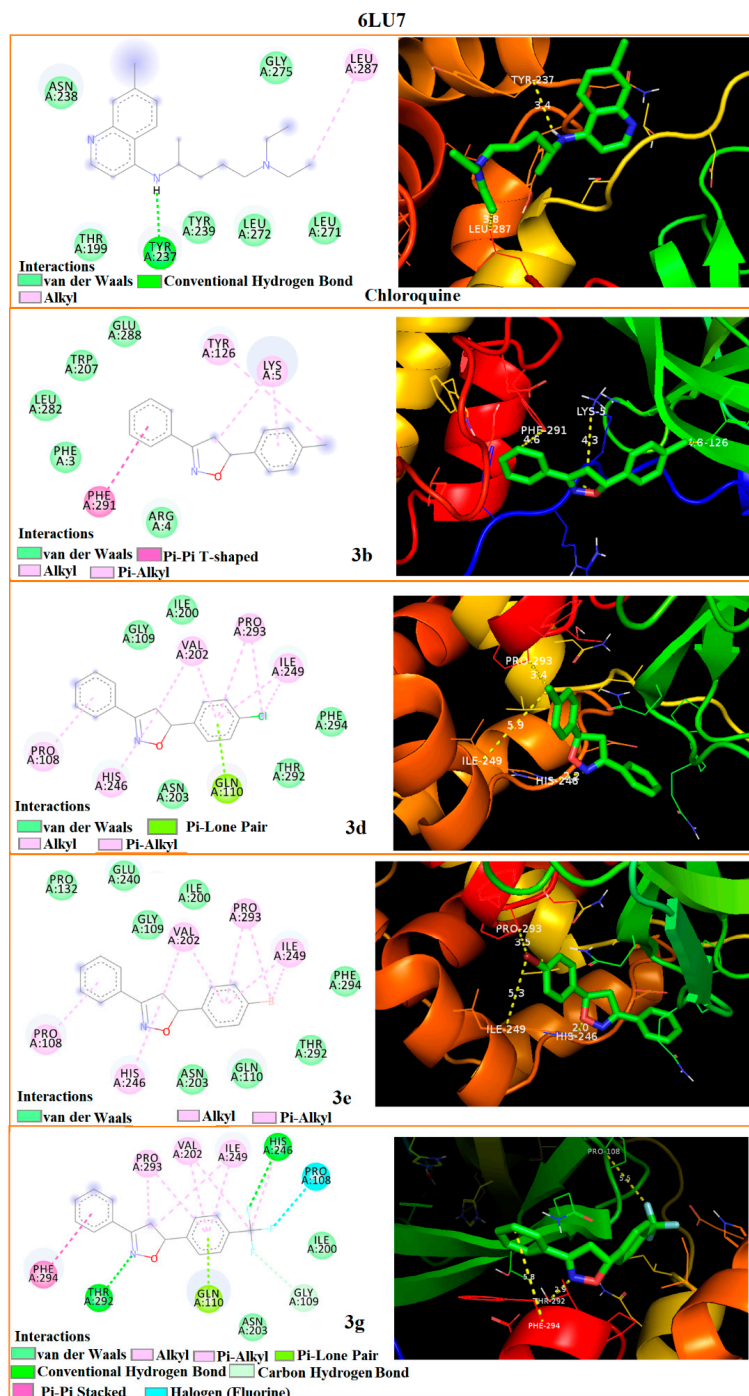
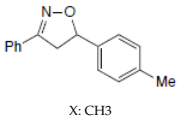
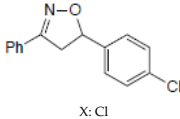
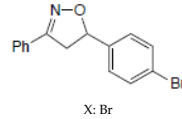
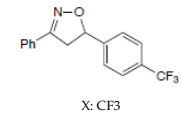
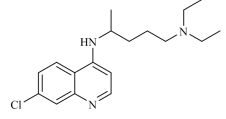
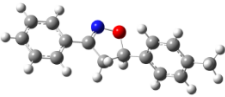
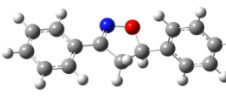
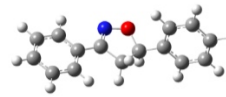
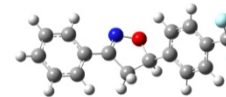
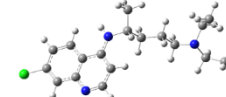


Figure 6. Binding orientation and molecular interactions of the studied D-m, C-m, B-m, A-m compounds into the active sites of 6LU7.

Table 2. Molecular docking results of the studied compounds and chloroquinein comparison.

Name	5-(<i>p</i> -methylphenyl)-3-phenyl-2-isoxazoline (D-m)			5-(<i>p</i> -chlorophenyl)-3-phenyl-2-isoxazoline (C-m)			5-(<i>p</i> -bromophenyl)-3-phenyl-2-isoxazoline (B-m)			3-phenyl-5-(<i>p</i> -trifluoromethyl-phenyl)-2-isoxazoline (A-m)			Chloroquine			
2D Compound Structure																
3D Compound Structure																
Binding Energy (kcal·mol ⁻¹)	5R7Y	-6.91			-6.98			-7.03			-6.63			-6.28		
	6LU7	-5.59			-6.21			-6.41			-5.99			-4.36		
Inhibition constant (μM)	5R7Y	8.62			7.64			7.03			13.79			24.95		
	6LU7	79.42			28.07			19.97			41.01			634.41		
Intermolecular energy (kcal·mol ⁻¹)	5R7Y	-7.51			-7.58			-7.63			-7.53			-8.67		
	6LU7	-6.19			-6.81			-7.01			-6.88			-6.75		
Interaction Residues-Bond distances (Å)	5R7Y	ARG-4 2.0	LYS-5 4.2	GLU-288 4.7	ARG-4 1.9	LYS-5 4.2	GLU-288 4.4	ARG-4 1.9	LYS-5 4.4	GLU-288 4.2	ARG-4 1.9	LYS-5 5.1	TYR-126 2.9	PHE-3 3.6	LYS-5 3.3	PHE-291 3.4
	6LU7	TYR-126 4.6	LYS-5 4.3	PHE-291 4.6	HIS-246 2.2	PRO-293 3.4	ILE-249 5.9	HIS-246 2.0	PRO-293 3.5	ILE-249 5.3	THR-292 2.9	PHE-294 5.8	PRO-108 5.5	TYR-237 3.4	LEU-287 3.8	-

4. Conclusions

The 32CA reactions of BrVB **1** and CIVB **2** with BzNO **3** were investigated in MEDT through DFT calculations at computational level B3LYP/6-311++G(d,p). Due to the non-symmetry of the reagents, two competitive regioisomeric reaction paths are feasible. The two regioisomeric reaction paths were studied. Exploration of the reaction and activation energies related with the two regioisomeric reaction paths designates that these 32CA reactions are totally regioselective, in clear agreement with the experimental results. ELF analysis along the more favorable *meta* reaction paths shows that these *zw-type* 32CA reactions begin with the formation of the single bond C-C, whereas the formation of the second C-O single bond takes place at the end of the reactions, thus characterizing the mechanism of these 32CA reactions as a non-concerted *two-stage one-step* one. Finally, docking studies on the resulting 2-isoxazolines to assess their efficacy and interaction for inhibition of SARS-CoV-2, shows that 5-(*p*-bromophenyl)-3-phenyl-2-isoxazoline **B-m** has greater interaction for the inhibition of SARS-CoV-2 than the other studied 2-isoxazolines.

Supplementary Materials: The following are available online at <https://www.mdpi.com/2673-401X/2/1/1/s1>, Tables including B3LYP/6-311++G(d,p) total and relative electronic energies, in gas phase and in THF, and B3LYP/6-31G(d,p) thermodynamic data, computed at 25 °C and 1 atm in THF, for the stationary points involved in the 32CA reaction of BrVB **1** and CIVB **2** with BzNO **3**, BET of the C-C and C-O bond formation along the 32CA reaction of BrVB **1** and CIVB **2** with BzNO **3** and Cartesian coordinates and electronic energies for TSs structures, reactants and products together with the single imaginary frequencies of the TSs.

Author Contributions: Conceptualization, L.R.D.; H.E.A.E.A. Data curation, A.Z. Formal analysis, N.M., M.E.I.; Funding acquisition, M.E.G.; Investigation, A.Z.; M.S.; A.O.A., M.R.-G. and A.E. Methodology, A.O.A. Resources, A.Z.; Supervision, M.S., M.E.I. Writing original draft, A.Z.; N.M. Writing—review & editing, A.Z. All authors have read and agreed to the published version of the manuscript.

Funding: This research was supported by the MENFPESRS-DESRS and UCD. LRD is grateful to the Ministerio de Ciencias e Innovación (MICINN) of the Spanish Government for the project PID2019-110776GB-I00 (AEI/FEDER, UE). This project has also received funding from the European Union's Horizon 2020 research and innovation programme under the Marie Skłodowska-Curie grant agreement No. 846181 (MRG).

Conflicts of Interest: The authors declare no conflict of interest.

References

1. Southon, I.W.; Buckingham, J. *Dictionary of Alkaloids*; Chapman & Hall: New York, NY, USA, 1989.
2. Gothelf, K.V.; Jørgensen, K.A. Asymmetric 1,3-Dipolar Cycloaddition Reactions. *Chem. Rev.* **1998**, *98*, 863–910. [[CrossRef](#)]
3. Huisgen, R. Kinetics and Mechanism of 1,3-Dipolar Cycloadditions. *Angew. Chem. Int. Ed.* **1963**, *2*, 633–645. [[CrossRef](#)]
4. Huisgen, R. 1,3-Dipolar cycloadditions. 76. Concerted nature of 1,3-dipolar cycloadditions and the question of diradical intermediates. *J. Org. Chem.* **1976**, *41*, 403–419. [[CrossRef](#)]
5. Firestone, R.A. Mechanism of 1,3-dipolar cycloadditions. *J. Org. Chem.* **1968**, *33*, 2285–2290. [[CrossRef](#)]
6. Firestone, R.A. The diradical mechanism for 1,3-dipolar cycloadditions and related thermal pericyclic reactions. *Tetrahedron* **1977**, *33*, 3009–3039. [[CrossRef](#)]
7. Firestone, R.A. The Low Energy of Concert in Many Symmetry Allowed Cycloadditions Supports a Stepwise Diradical Mechanism. *Int. J. Chem. Kinet.* **2013**, *45*, 415–428. [[CrossRef](#)]
8. Kozikowski, A.P. The isoxazoline route to the molecules of nature. *Acc. Chem. Res.* **1984**, *17*, 410–416. [[CrossRef](#)]
9. Kumar, A.B.V.K.; Sankar, A.U.R.; Kim, S.H. A Simple, Efficient One Pot Synthesis of 2-Isoxazoline Derivatives and their Antimicrobial Activity. *J. Heterocycl. Chem.* **2014**, *51*, E146–E151. [[CrossRef](#)]
10. Diana, G.D.; McKinlay, M.A.; Brisson, C.J.; Zalay, E.S.; Miralles, J.V.; Salvador, U.J. Isoxazoles with anti-picornavirus activity. *J. Med. Chem.* **1985**, *28*, 748–752. [[CrossRef](#)] [[PubMed](#)]
11. Antczak, C.; Bauvois, B.; Monneret, C.; Florent, J.C. A new acivicin prodrug designed for tumor-Targeted delivery. *Bioorg. Med. Chem.* **2001**, *9*, 2843–2848. [[CrossRef](#)]
12. Prajapati, S.K.; Shrivastava, S.; Bihade, U.; Gupta, A.K.; Naidu, V.G.M.; Banerjee, U.C.; Babu, B.N. Synthesis and biological evaluation of novel Δ^2 -isoxazoline fused cyclopentane derivatives as potential antimicrobial and anticancer agents. *Med. Chem. Comm.* **2015**, *6*, 839–845. [[CrossRef](#)]

13. Zhang, P.; Wei, C.; Wang, E.; Wang, W.; Liu, M.; Yin, Q.; Chen, H.; Wang, K.; Li, X.; Zhang, J. Synthesis and biological activities of novel isoxazoline-linked pseudodisaccharide derivatives. *Carbohydr. Res.* **2012**, *351*, 7–16. [[CrossRef](#)] [[PubMed](#)]
14. Abdelall, E.K.A. Synthesis and biological evaluations of novel isoxazoles and furoxan derivative as anti-inflammatory agents. *Bioorg. Chem.* **2019**, *94*, 103441. [[CrossRef](#)]
15. Zhu, J.; Mo, J.; Lin, H.-Z.; Chen, Y.; Sun, H.-P. The recent progress of isoxazole in medicinal chemistry. *Bioorg. Med. Chem.* **2018**, *26*, 3065–3075. [[CrossRef](#)]
16. Zadrozna, I.; Kurkowska, J.; Kruszewska, H.; Makuch, I. 4,5-Dihydroisoxazoles: Testing of antimicrobial activity. *Il Farmaco.* **2000**, *55*, 499–501. [[CrossRef](#)]
17. Liu, X.; Lu, D.; Wu, J.-H.; Tan, J.-P.; Jiang, C.; Gao, G.; Wang, T. Stereoselective Synthesis of CF₃-Containing Spiro oxindoles via 1,3-Dipolar Cycloaddition by Dipeptide Based Phosphonium Salt Catalysis. *Adv. Synth. Catal.* **2020**, *362*, 1490–1495. [[CrossRef](#)]
18. Gui, H.-Z.; Wei, Y.; Shi, M. Recent Advances in the Construction of Trifluoromethyl Containing Spiro oxindoles through Cycloaddition Reactions. *Chem. Asian J.* **2020**, *15*, 1225–1233. [[CrossRef](#)]
19. Uno, H.; Imai, T.; Harada, K.; Shibata, N. Synthesis of Highly Functionalized 12-Membered Trifluoromethyl Heterocycles via a Nonde carboxyl ative Pd-Catalyzed [6 + 6] Annulation. *ACS Catal.* **2020**, *10*, 1454–1459. [[CrossRef](#)]
20. Bigelow, L.A. The Action of Elementary Fluorine upon Organic Compounds. *Chem. Rev.* **1947**, *40*, 51–115. [[CrossRef](#)]
21. Yoshimura, A.; Zhdankin, V.V. Advances in Synthetic Applications of Hypervalent Iodine Compounds. *Chem. Rev.* **2016**, *116*, 3328–3435. [[CrossRef](#)]
22. Muller, K.; Faeh, C.; Diederich, F. Fluorine in Pharmaceuticals: Looking Beyond Intuition. *Science* **2007**, *317*, 1881–1886. [[CrossRef](#)]
23. Aggarwal, R.; Bansal, A.; Mittal, A. Synthesis and antimicrobial activity of 3-(2-thienyl)-4-aryloxy-5-hydroxy-5-trifluoromethyl- Δ^2 -isoxazolines and 3-(2-thienyl)-4-aryloxy-5-trifluoromethylisoxazoles. *J. Fluor. Chem.* **2013**, *145*, 95–101. [[CrossRef](#)]
24. Filler, R.; Kobayashi, Y. *Biomedical Aspects of Fluorine Chemistry*; Elsevier: New York, NY, USA, 1982.
25. Giovannoni, M.P.; Vergelli, C.; Ghelardini, C.; Galeotti, N.; Bartolini, A.; Piaz, V.D. [(3-Chlorophenyl)piperazinylpropyl]pyridazinones and Analogues as Potent Antinociceptive Agents. *J. Med. Chem.* **2003**, *46*, 1055–1059. [[CrossRef](#)]
26. Karthikeyan, K.; Seelan, T.V.; Lalitha, K.G.; Perumal, P.T. Synthesis and antinociceptive activity of pyrazolyl isoxazolines and pyrazolyl isoxazoles. *Bioorg. Med. Chem. Lett.* **2009**, *19*, 3370–3373. [[CrossRef](#)]
27. Kamal, A.; Bharathi, E.V.; Reddy, J.S.; Ramaiah, M.J.; Dastagiri, D.; Reddy, M.K.; Viswanath, A.; Reddy, T.L.; Shaik, T.B.; Pushpavalli, S.N.C.V.L.; et al. Synthesis and biological evaluation of 3,5-diaryl isoxazoline/isoxazole linked 2,3-dihydroquinazolinone hybrids as anticancer agents. *Eur. J. Med. Chem.* **2011**, *46*, 691–703. [[CrossRef](#)]
28. Patrizia, D.; Carbone, A.; Barraja, P.; Kelter, G.; Fiebig, H.H.; Cirrincione, G. Synthesis and antitumor activity of 2,5-bis(3'-indolyl)-furans and 3,5-bis(3'-indolyl)-isoxazoles, nortopsentin analogues. *Bioorg. Med. Chem.* **2010**, *18*, 4524–4529.
29. Isanbor, C.; O'Hagan, D. Fluorine in medicinal chemistry: A review of anti-cancer agents. *J. Fluor. Chem.* **2006**, *127*, 303–319. [[CrossRef](#)]
30. De Weerd, N.J.; Bukovsky, E.V.; Castro, P.K.; Kuvychko, I.V.; Popovb, A.A.; Strauss, S.H.; Olga Boltalina, V. Steric and electronic effects of CF₃ conformations in acene(CF₃)_n derivatives. *J. Fluor. Chem.* **2019**, *221*, 1–7. [[CrossRef](#)]
31. Haranahalli, K.; Honda, T.; Ojima, I. Recent progress in the strategic incorporation of fluorine into medicinally active compounds. *J. Fluor. Chem.* **2019**, *217*, 29–40. [[CrossRef](#)]
32. Agbaje, C.O.; Fadeyi, O.O.; Okoro, O.C. Lewis acid mediated diastereoselective synthesis of fused fluorinated spiroketal as potential biologically active compounds. *Tetrahedron Lett.* **2011**, *52*, 5297–5300. [[CrossRef](#)]
33. Jbeily, M.; Kressler, J. Fluorophilicity and lipophilicity of fluorinated rhodamines determined by their partition coefficients in biphasic solvent systems. *J. Fluor. Chem.* **2017**, *193*, 67–72. [[CrossRef](#)]
34. Ojima, I. *Fluorine in Medicinal Chemistry and Chemical Biology*; Wiley-Blackwell: Chichester, UK, 2009.
35. Wang, J.; Sánchez-Roselló, M.; Aceña, J.L.; del Pozo, C.; Sorochinsky, A.E.; Fustero, S.; Soloshonok, V.A.; Liu, H. Fluorine in Pharmaceutical Industry: Fluorine-Containing Drugs Introduced to the Market in the Last Decade (2001–2011). *Chem. Rev.* **2014**, *114*, 2432–2506. [[CrossRef](#)] [[PubMed](#)]
36. Koldobskii, A.B.; Shilova, O.S.; Artyushin, O.I.; Kagramanov, N.D.; Moiseev, S.K. Polyfluorinated esters of 4-chloro-2-oxobut-3-ynoic acid. Cycloaddition reactions of hexafluoro isopropyl 4-chloro-2-oxobut-3-ynoate, an incredibly electrophilic alkyne. *J. Fluor. Chem.* **2020**, *231*, 109463. [[CrossRef](#)]
37. Bigotti, S.; Malpezzi, L.; Molteni, M.; Mele, A.; Panzeri, W.; Zanda, M. Functionalized fluoroalkyl heterocycles by 1,3-dipolar cycloadditions with γ -fluoro- α -nitroalkenes. *Tetrahedron Lett.* **2009**, *50*, 2540–2542. [[CrossRef](#)]
38. O'Hagan, D. Fluorine in health care: Organofluorine containing blockbuster drugs. *J. Fluor. Chem.* **2010**, *131*, 1071–1081. [[CrossRef](#)]
39. McGrath, N.A.; Brichacek, M.; Njardarson, J.T.A. Graphical Journey of Innovative Organic Architectures That Have Improved Our Lives. *J. Chem. Educ.* **2010**, *87*, 1348–1349. [[CrossRef](#)]
40. Zhou, Y.; Wang, J.; Gu, Z.; Wang, S.; Zhu, W.; Aceña, J.L.; Soloshonok, V.A.; Izawa, K.; Liu, H. Next Generation of Fluorine-Containing Pharmaceuticals, Compounds Currently in Phase II–III Clinical Trials of Major Pharmaceutical Companies: New Structural Trends and Therapeutic Areas. *Chem. Rev.* **2016**, *116*, 422–518. [[CrossRef](#)]
41. Domingo, L.R. Molecular Electron Density Theory: A Modern View of Reactivity in Organic Chemistry. *Molecules* **2016**, *21*, 1319. [[CrossRef](#)]
42. Ríos-Gutiérrez, M.; Domingo, L.R. Unravelling the Mysteries of the [3 + 2] Cycloaddition Reactions. *Eur. J. Org. Chem.* **2019**, *2019*, 267–282. [[CrossRef](#)]

43. Domingo, L.R.; Aurell, M.J.; Pérez, P. A DFT analysis of the participation of zwitterionic TACs in polar [3 + 2] cycloaddition reactions. *Tetrahedron* **2014**, *70*, 4519–4525. [[CrossRef](#)]
44. Zeroual, A.; Ríos-Gutiérrez, M.; El Idrissi, M.; El Alaoui El Abdallaoui, H.; Domingo, L.R. An MEDT study of the mechanism and selectivities of the [3 + 2] cycloaddition reaction of tomentosin with benzonitrile oxide. *Int. J. Quantum Chem.* **2019**, *119*, e25980. [[CrossRef](#)]
45. Zeroual, A.; Ríos-Gutiérrez, M.; Salah, M.; El Alaoui El Abdallaoui, H.; Domingo, L.R. An investigation of the molecular mechanism, chemoselectivity and regioselectivity of cycloaddition reaction between acetonitrile N-Oxide and 2,5-dimethyl-2H-[1,2,3]diazaphosphole: A MEDT study. *J. Chem. Sci.* **2019**, *131*, 75. [[CrossRef](#)]
46. Yoshimura, A.; Middleton, K.R.; Todora, A.D.; Kastern, B.J.; Koski, S.R.; Maskaev, A.V.; Zhdankin, V.V. Hypervalent Iodine Catalyzed Generation of Nitrile Oxides from Oximes and their Cycloaddition with Alkenes or Alkynes. *Org. Lett.* **2013**, *15*, 4010–4013. [[CrossRef](#)] [[PubMed](#)]
47. Becke, A.D. Density-functional thermochemistry. III. The role of exact exchange. *J. Chem. Phys.* **1993**, *98*, 5648–5652. [[CrossRef](#)]
48. Hehre, W.J.; Radom, L.; Schleyer, P.R.; Pople, J.A. *Ab Initio Molecular Orbital Theory*; Wiley: New York, NY, USA, 1986.
49. Fisch, M.J.; Trucks, G.W.; Schlegel, H.B.; Scuseria, G.E.; Robb, M.A.; Cheeseman, J.R.; Scalmani, G.; Barone, V.; Petersson, G.A.; Nakatsuji, H.; et al. *Gaussian 09, Revision A.02*; Fox, Gaussian, Inc.: Wallingford, CT, USA, 2016.
50. Schlegel, H.B. Optimization of equilibrium geometries and transition structures. *J. Comput. Chem.* **1982**, *3*, 214–218. [[CrossRef](#)]
51. Fukui, K. Formulation of the reaction coordinate. *J. Phys. Chem.* **1970**, *74*, 4161–4163. [[CrossRef](#)]
52. Gonzalez, C.; Schlegel, H.B. Improved algorithms for reaction path following: Higher order implicit algorithms. *J. Chem. Phys.* **1991**, *95*, 5853–5860. [[CrossRef](#)]
53. Tomasi, J.; Persico, M. Molecular Interactions in Solution: An Overview of Methods Based on Continuous Distributions of the Solvent. *Chem. Rev.* **1994**, *94*, 2027–2094. [[CrossRef](#)]
54. Barone, V.; Cossi, M.; Tomasi, J. Geometry optimization of molecular structures in solution by the polarizable continuum model. *J. Comput. Chem.* **1998**, *19*, 404–417. [[CrossRef](#)]
55. Domingo, L.R. A new C–C bond formation model based on the quantum chemical topology of electron density. *RSC Adv.* **2014**, *4*, 32415–32428. [[CrossRef](#)]
56. Reed, A.E.; Curtiss, L.A.; Weinhold, F. Intermolecular interactions from a natural bond orbital, donor-acceptor viewpoint. *Chem. Rev.* **1988**, *88*, 899–926. [[CrossRef](#)]
57. Domingo, L.R.; Ríos-Gutiérrez, M.; Pérez, P. Applications of the Conceptual Density Functional Theory Indices to Organic Chemistry Reactivity. *Molecules* **2016**, *21*, 748. [[CrossRef](#)] [[PubMed](#)]
58. Becke, A.D.; Edgecombe, K.E. A simple measure of electron localization in atomic and molecular systems. *J. Chem. Phys.* **1990**, *92*, 5397–5403. [[CrossRef](#)]
59. Noury, S.; Krokidis, X.; Fuster, F.; Silvi, B. Computational tools for the electron localization function topological analysis. *Comput. Chem.* **1999**, *23*, 597–604. [[CrossRef](#)]
60. Krokidis, X.; Noury, S.; Silvi, B. Characterization of Elementary Chemical Processes by Catastrophe Theory. *J. Phys. Chem. A* **1997**, *101*, 7277–7282. [[CrossRef](#)]
61. Lefebvre, C.; Khartabil, H.; Boisson, J.C.; Garcia, J.C.; Piquemal, J.P.; Hénon, E. The Independent Gradient Model: A New Approach for Probing Strong and Weak Interactions in Molecules from Wave Function Calculations. *Chem. Phys. Chem.* **2018**, *19*, 724–735. [[CrossRef](#)]
62. Görling, A. Density-functional theory beyond the Hohenberg-Kohn theorem. *Phys. Rev. A* **1999**, *59*, 3359–3374. [[CrossRef](#)]
63. Salah, M.; Belghiti, M.E.; Aitouna, A.O.; Zeroual, A.; Jorio, S.; El Alaoui, A.H.; El hadki, H.; Marakchi, K.; Komiha, N. MEDT study of the 1,3-DC reaction of diazomethane with Psilostachyin and investigation about the interactions of some pyrazoline derivatives with protease (Mpro) of nCoV-2. *J. Mol. Graph. Model.* **2021**, *102*, 107763. [[CrossRef](#)]
64. Lu, T.; Chen, F. Multiwfn: A multifunctional wave function analyzer. *J. Comput. Chem.* **2012**, *33*, 580–592. [[CrossRef](#)]
65. Silvi, B.; Savin, A. Classification of chemical bonds based on topological analysis of electron localization functions. *Nature* **1994**, *371*, 683–686. [[CrossRef](#)]
66. Parr, R.G.; Yang, W. *Density Functional Theory of Atoms and Molecules*; Oxford University Press: New York, NY, USA, 1989.
67. Parr, R.G.; Szentpaly, L.V.; Liu, S. Electrophilicity Index. *J. Am. Chem. Soc.* **1999**, *121*, 1922–1924. [[CrossRef](#)]
68. Domingo, L.R.; Chamorro, E.; Pérez, P. Understanding the Reactivity of Captodative Ethylenes in Polar Cycloaddition Reactions. A Theoretical Study. *J. Org. Chem.* **2008**, *73*, 4615–4624. [[CrossRef](#)] [[PubMed](#)]
69. Aurell, M.J.; Domingo, L.R.; Pérez, P.; Contreras, R. A theoretical study on the regioselectivity of 1,3-dipolar cycloadditions using DFT-based reactivity indexes. *Tetrahedron* **2004**, *60*, 11503–11509. [[CrossRef](#)]
70. Domingo, L.R.; Ríos-Gutiérrez, M.; Castellanos Soriano, J. Understanding the Origin of the Regioselectivity in Non-Polar [3 + 2] Cycloaddition Reactions through the Molecular Electron Density Theory. *Org. Chem.* **2020**, *1*, 3. [[CrossRef](#)]
71. Domingo, L.R.; Pérez, P.; Sáez, J.A. Understanding the local reactivity in polar organic reactions through electrophilic and nucleophilic Parr functions. *RSC Adv.* **2013**, *3*, 1486–1494. [[CrossRef](#)]
72. Zeroual, A.; Ríos-Gutiérrez, M.; El Ghozlani, M.; El Idrissi, M.; OuledAitouna, A.; Salah, M.; El Abdallaoui, H.E.; Domingo, L.R. A molecular electron density theory investigation of the molecular mechanism, regioselectivity, stereoselectivity and chemoselectivity of cycloaddition reaction between acetonitrile N-oxide and 2,5-dimethyl-2H-[1,2,3]diazarsole. *Theor. Chem. Acc.* **2020**, *139*, 37. [[CrossRef](#)]

73. Domingo, L.R.; Sáez, J.A.; Zaragoza, R.J.; Arnó, M. Understanding the Participation of Quadricyclane as Nucleophile in Polar Cycloadditions toward Electrophilic π Molecules. *J. Org. Chem.* **2008**, *73*, 8791–8799. [[CrossRef](#)]
74. Didelot, C.; Lanneau, D.; Brunet, M.; Joly, A.L.; Thonel, A.D.; Chiosis, G.; Garrido, C. Anti-Cancer Therapeutic Approaches Based on Intracellular and Extracellular Heat Shock Proteins. *Curr. Med. Chem.* **2007**, *14*, 2839–2847. [[CrossRef](#)]
75. Tumma, R.; Vamaraju, H.B. Design, Synthesis, Molecular Docking, and Biological Evaluation of Pyrazole 1-Carbothiamide incorporated Isoxazole Derivatives. *Asian J. Pharm. Clin. Res.* **2019**, *12*, 245–250. [[CrossRef](#)]
76. Loh, B.; Vozzolo, L.; Mok, B.J.; Lee, C.C.; Fitzmaurice, R.J.; Caddick, S.; Fassati, A. Inhibition of HIV-1 Replication by Isoxazolidine and Isoxazole Sulfonamides. *Chem. Biol. Drug. Des.* **2010**, *75*, 461–474. [[CrossRef](#)]
77. Panda, S.S.; Chowdary, P.V.; Jayashree, B.S. Synthesis, Antiinflammatory and Antibacterial Activity of Novel Indolyl-isoxazoles. *Indian J. Pharm. Sci.* **2009**, *71*, 684–687. [[CrossRef](#)]
78. Durgamma, S.; Reddy, P.R.; Padmavathi, V.; Padmaja, A. Synthesis and Antioxidant Activity of Amido-Linked Benzoxazolyl/Benzothiazolyl/BenzimidazolylPyrazoles and Isoxazoles. *J. Heterocycl. Chem.* **2016**, *53*, 738–747. [[CrossRef](#)]
79. Makarov, V.A.; Riabova, O.B.; Granik, V.G.; Wutzler, P.; Schmidtke, M. Novel [(biphenyloxy)propyl]isoxazole derivatives for inhibition of human rhinovirus 2 and coxsackie virus B3 replication. *J. Antimicrob. Chemother.* **2005**, *55*, 483–488. [[CrossRef](#)]
80. Basha, S.S.; Divya, K.; Padmaja, A.; Padmavathi, V. Synthesis and antimicrobial activity of thiazolyl pyrazoles and isoxazoles. *Res. Chem. Int.* **2015**, *41*, 10067–10083. [[CrossRef](#)]
81. Arrieta, A.; Carrillo, J.R.; Cossio, F.P.; Diaz-Ortiz, A.; Gomez-Escalonilla, M.J.; Hoz, A.D.L.; Langa, F.; Moreno, A. Efficient tautomerization hydrazone-azomethine imine under microwave irradiation. Synthesis of [4,3'] and [5,3']bipyrazoles. *Tetrahedron* **1998**, *54*, 13167–31180. [[CrossRef](#)]
82. Berman, H.M.; Westbrook, J.; Feng, Z.; Gilliland, G.; Bhat, T.N.; Weissig, H.; Shindyalov, I.N.; Bourne, P.E. The Protein Data Bank. *Nucleic Acids Res.* **2000**, *28*, 235–242. [[CrossRef](#)]
83. Burley, S.K.; Berman, H.M.; Bhikadiya, C.; Bi, C.; Chen, L.; Costanzo, L.D.; Feng, Z. RCSB Protein Data Bank: Biological macromolecular structures enabling research and education in fundamental biology, biomedicine, biotechnology and energy. *Nucleic Acids Res.* **2019**, *47*, D464–D474. [[CrossRef](#)]
84. Goodsell, D.S.; Olson, A.J. Automated Docking of Substrates to Proteins by Simulated Annealing. *Proteins Struct. Funct. Bioinform.* **1990**, *8*, 195–202. [[CrossRef](#)] [[PubMed](#)]
85. Morris, G.M.; Goodsell, D.S.; Halliday, R.S.; Huey, R.; Hart, W.E.; Belew, R.K.; Olson, A.J. Automated docking using a Lamarckian genetic algorithm and an empirical binding free energy function. *J. Comput. Chem.* **1998**, *19*, 1639–1662. [[CrossRef](#)]
86. Katritzky, A.R.; Mu, L.; Lobanov, V.S.; Karelson, M. Correlation of Boiling Points with Molecular Structure. 1. A Training Set of 298 Diverse Organics and a Test Set of 9 Simple Inorganics. *J. Phys. Chem.* **1996**, *100*, 10400–10407. [[CrossRef](#)]
87. Solis, F.J.; Wets, R.J.B. Minimization by Random Search Techniques. *Math. Oper. Res.* **1981**, *6*, 19–30. [[CrossRef](#)]